Journal of Colloid and Interface Science 645 (2023) 502–512

Contents lists available at ScienceDirect

Journal of Colloid And Interface Science

journal homepage: www.elsevier.com/locate/jcis

Synthesis of patterned polyHIPE-hydrogel composite materials using thiol-ene chemistry

Tucker J. McKenzie, Christian Cawood, Chelsea Davis, Neil Ayres *

Department of Chemistry, The University of Cincinnati, P.O. Box 210172, Cincinnati, OH 45221, United States

GRAPHICAL ABSTRACT

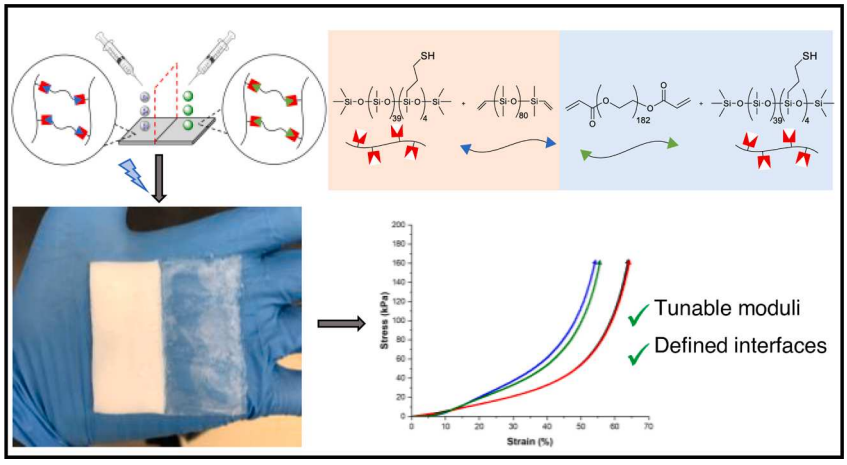

ARTICLE INFO

Keywords:
Interface stability
Emulsion templated polymer
Patterned materials
PolyHIPE

ABSTRACT

Elastomeric materials combining multiple properties within a single composite are highly desired in applications including biomaterials interfaces, actuators, and soft robotics. High spatial resolution is required to impart different properties across the composite for the intended application, but many techniques used to prepare these composites rely on multistep and complex methods. There is a need for the development of simple and efficient platforms to design layered composite materials. Here, we report the synthesis of horizontally- and vertically-patterned composites consisting of PDMS-based polymerized high internal phase emulsion (polyHIPE) porous elastomers and PDMS/PEG hydrogels. Composites with defined interfaces that were mechanically robust were prepared, and rheological analysis of the polyHIPE and hydrogel layers showed storage moduli values of ~ 35 kPa and 45 kPa respectively. The compressive Young's Modulus and maximum strain of the polyHIPEs were dependent on the thiol to ene ratio in the formulation and obtained values ranging from 6 to 25 kPa and 50–65% respectively. The mechanical properties, total porosity of the polyHIPE, and swelling ratio of the hydrogel were unaffected by the patterning technique compared to non-patterned controls. PolyHIPE-hydrogel composite

* Corresponding author.
E-mail address: neil.ayres@uc.edu (N. Ayres).

https://doi.org/10.1016/j.jcis.2023.04.132
Received 10 February 2023; Received in revised form 17 April 2023; Accepted 24 April 2023
Available online 4 May 2023

materials having up to 7-different horizontally pattered layers could be prepared that could expand and contract up hydration and drying.

1. Introduction

Elastomers that combine different materials within a single composite have been shown to be useful in many areas, including biomimetic tissue scaffolds,[1-5] water purification materials,[6,7] stimuli responsive actuators,[8,9] and soft robotics.[10] Many of these applications rely on high spatial resolution of the two or more different materials. For example, in stimuli responsive actuators, the size and shape of responsive layers dictate the direction or magnitude of motion.[11] This was demonstrated by Bertoldi and coworkers,[8] where the design parameters of fiber-elastomer segments in a Kevlar wrapped silicone elastomer could control bending, twisting, or expansion motion under fluid pressure to mimic the complex motion of fingers. Similarly, controlling bulk morphology properties, including porosity, in a patterned fashion is desirable for biomimetic tissue scaffolds to better model the complicated native bone-tendon interfaces.[3,12-14] Porous elastomers are used in application including flexible sensors,[15,16] absorbents,[17,18] and biomaterials.[19,20] For example, Cho and coworkers[13] showed that preparing a porous collagen-based scaffold with a gradient in chemistry and pore size provided enhanced cell proliferation in the hydrogel "tendon" layer compared to the "bone" layer where human osteoblasts proliferated. Their results showed that cell behavior was dependent upon the microenvironment of each layer within a single 3D scaffold. However, many examples use complex or multistep synthesis methods to prepare materials having layers of differing properties while maintaining spatial resolution.

Hydrogels are water-swollen polymeric materials that are among the mostly widely studied biomaterials.[21,22] Specifically, elastomeric hydrogels are able to provide the water content, toughness, and compressive strength, etc. to prepare synthetic cartilage[23-26] and tendon.[27,28] Hydrogels with desirable elastic properties can be prepared using polymer networks having both hydrophilic and hydrophobic components.[29-31] The introduction of hydrophobic components into the hydrogel network can improve the elasticity of polymeric gels. For example, Crosby, Tew, and coworkers[29] showed a hydrogel consisting of a norbornene end-functionalized poly(ethylene glycol) (PEG) and polydimethylsiloxane (PDMS) showed excellent mechanical resilience (97% efficiency at 300% strain) and that the volume fraction of PDMS in the gel could tune the water content and Young's modulus.

One way to produce porous polymers is using an emulsion templating technique called polymerized high internal phase emulsions (polyHIPE).[32-34] The pore size, pore morphology, and mechanical properties of polyHIPEs can be readily tuned and are dependent on the preparation conditions and the composition of the pre-polymerized emulsion.[35] PolyHIPEs can be prepared from thermal free radical polymerizations [36-38] or UV initiated orthogonal coupling "click" reactions,[39-43] in particular thiol-ene reactions.[44-52] The properties of thiol-ene polyHIPEs can be modified or controlled by the chemistry and the molar stoichiometric ratio of the thiol- and ene-containing components. For example, Claeyssens and coworkers [45] introduced biodegradability into a polyHIPE network using three-arm and four-arm methacrylate-functionalized polycaprolactones that showed comparable human osteosarcoma cell viability and spreading over a 7-day period on polyHIPEs having four-arm PCL networks compared to tissue culture polystyrene. Our lab has prepared PDMS-based polyHIPEs using thiol- and ene-functionalized PDMSs where the thiol to ene ratio was used to control the storage moduli at a single total porosity.[47,48] In addition to the wide library of compatible monomers available for polymerization, UV initiated thiol-ene reactions can prepare polymeric materials with multiple layers having distinct properties in each layer.[53,54] The orthogonal nature of thiol-ene reactions allows for covalent bonding to occur between deposited layers ensuring a robust interface is produced. Layered hydrogels[55-58] and layered polyHIPEs[59,60] have been prepared where the rapid polymerization rate of thiol-ene reactions, along with the viscosity of the precursor solutions, are recognized as key factors in maintaining the defined interface between layers.

In the work described here, we have prepared a series of patterned PDMS-based composite materials with alternating layers of polyHIPE and hydrogel together with high spatial resolution. Horizontally layered- and vertically stacked-polyHIPE-hydrogel composite materials (H-PH-HGs or S-PH-HGs) were synthesized using a simple emulsion and hydrogel patterning processes followed by a single curing step, shown in Fig. 1.

We varied the ratio of thiol- to ene-containing PDMSs in the polyHIPEs, as this has been proven to be a key parameter to tune the storage modulus, and we varied the solids content in the hydrogels as this is a simple way to tune the swelling ratio and dynamic moduli. Throughout this manuscript we describe the emulsion templated materials as poly*HIPEs* even though the volume fraction of dispersed phase used to prepare them were below the accepted value of 74% for simplicity in naming and comparison across other literature.

2. Experimental

2.1. Materials

The photoinitiator 2,2-Dimethoxy-2-phenylacetophenone (DMPA), reagent grade solvents dichloromethane (DCM), tetrahydrofuran (THF), and methanol (MeOH), poly(ethylene glycol)-8000, and acryloyl chloride were purchased from Sigma-Aldrich (St. Louis, MO, USA). The polymers [13–17% (mercaptopropyl) methylsiloxane]–dimethylsiloxane copolymer (thiolated-PDMS), vinyl terminated polydimethylsiloxane (vinyl-PDMS), and (30–35% dodecylmethylsiloxane-[7–10% hydroxy(propethyleneoxy (6–9) propyl) methylsiloxane] –(55–65% dimethylsiloxane) terpolymer (Silube J208-812) were purchased from Gelest (Morrisville, PA, USA). Sodium Chloride (NaCl), triethylamine (TEA), sodium hydroxide (NaOH), hydrochloric acid (HCl), and diethyl ether, were purchased from Oakwood Chemical (Estill, SC, USA). All reagents and chemicals were used as received without any modifications.

2.2. Synthesis of PEG-8000-diacrylate (PEG-DA)

Hydroxy-terminated PEG (20.0 g, 2.5 mmol, M_n = 8,000 g/mol) was dissolved in DCM in a flame-dried round bottom flask equipped with a stir bar. An addition funnel containing triethyl amine (1.03 mL, 8.25 mmol) was fixed to the round bottom flask, sealed with a septum, and the flask was then cooled in an ice water bath. The triethyl amine was slowly added dropwise through the addition funnel and the mixture allowed to stir for 10 min. A solution of acryloyl chloride (0.606 mL, 7.5 mmol) in DCM was carefully prepared inside the addition funnel and then slowly added dropwise to the reaction mixture while stirring and left to proceed for 24 h. Excess acryloyl chloride was quenched by the addition of deionized water and left to stir for 10 min. The organic phase was washed extensively with a NaOH solution (0.5 M), HCl solution (0.5 M), deionized water, and brine and then dried over sodium sulfate. The organic layer was removed using a rotary-evaporator until a viscous oil was obtained. The concentrated solution was precipitated into cold diethyl ether, isolated, and further dried overnight in a vacuum oven at room temperature to yield 17.4 g (~87%) of a white powder. ^{1}H NMR (400 MHz, CDCl3) δ [ppm] = 6.43, 6.16, and 5.84 (m, 3H, CH_2CHC vinyl), 4.32 (m, 2H, $COCH_2CH_2$) 3.84–3.44 (m, 307H, OCH_2CH_2O) ^{13}C

NMR (101 MHz, $CDCl_3$) δ 166.13, 130.98, 128.29, 70.56, 69.11, 63.68 (Fig. S1).

2.3. Standard polyHIPE synthesis

PolyHIPEs were prepared using a modified procedure from our lab.[48] The continuous phase was first prepared in a 20 mL glass vial. Typically, for a polyHIPE with a 1:1 (thiol to alkene) functional group ratio, thiolated-PDMS (0.8 g, 0.914 mmol thiol-functional group), vinyl-PDMS (2.74 g, 0.914 mmol alkene-functional group), and Silube (36 mg, 1.0 wt% with respect to weight of continuous phase) were combined and vortexed. The photoinitiator DMPA (36 mg, 1.0 wt% with respect to weight of continuous phase) was dissolved in approximately 0.2 mL of DCM in a separate small glass vial. This solution was added to the continuous phase and vortexed until homogenous and protected from light. The dispersed phase (8.50 g, 70% v/v) consisting of a 1.5% wt/vol NaCl solution in Mili-Q water was added in small portions and vortexed until a viscous emulsion formed. The emulsion was poured into a mold and irradiated with UV light (λ_{max} = 365 nm) for 6 min in a mirrored enclosure and allowed to stand further for 5 min before being removed from the mold. PolyHIPEs were placed in the fume hood and dried for ~ 48 h at 22 °C. The final dried samples were characterized using scanning electron microscopy, density measurements and rheology.

2.4. Standard hydrogel synthesis

For a typical hydrogel with a 1:1 (thiol to ene) functional group ratio and 10 wt% solids content, the protocol was as follows: In a 20 mL glass vial, thiolated-PDMS (0.1 g, 0.114 mmol thiol-functional group) and PEG-DA (0.469 g, 0.114 mmol alkene-functional group) were dissolved in an 80/20 (v/v) THF/MeOH solution (5.6 g, 90 wt% with respect to total solids) using a vortex to stir. After the solids were dissolved, the photoinitiator DMPA (56 mg, 10 wt% with respect to total polymer content) was added and the vial was wrapped in aluminum foil. The organogel precursor solution was then transferred to a mold using a syringe equipped with a blunt needle and irradiated with UV light (λ_{max} = 365 nm) for 6 min in a mirrored enclosure, then immediately transferred to a beaker containing deionized water for 72 h with frequent water changes. After solvent exchange, the hydrogels were dried in a vacuum oven for ~ 48 h at 22 °C and weighed before being reswollen in deionized water for 48 h. The hydrogels were characterized using swelling ratio and gel fraction calculations and rheology in the swollen state.

2.5. PolyHIPE-hydrogel composites synthesis

Horizontal- and stacked-polyHIPE-hydrogel composites (H-PH-HGs or S-PH-HGs) were prepared using a modified emulsion patterning method adapted from previous work in our lab.[60] We first prepared the emulsion template as described in the Standard polyHIPE Synthesis. The emulsion was then transferred into a syringe. The hydrogel precursor solution was prepared as described in the Standard Hydrogel Synthesis section and transferred to a separate syringe. H- and S-PH-HGs were prepared by extruding the two solutions from the prepared syringes into molds in a stepwise process. For horizontal-PH-HGs, molds with a slight notch along the inner wall were used to allow for a thin divider to be placed separating the two layers. One side of the mold was filled with the emulsion first, and then the hydrogel precursor solution was added to fill the remaining half of the template (Fig. S2). The divider was slowly removed before placing the template under the UV light source (λ_{max} = 365 nm) for 6 min. For stacked-PH-HGs, a circular mold was first secured to a glass slide and then filled with the emulsion. Next, a second circular mold was placed directly on top of the first and filled with the hydrogel precursor solution. The emulsion and hydrogel were then irradiated with UV-light for 6 min. Following the UV initiated thiol-ene reactions, the materials were removed from the template and transferred to a beaker containing deionized water for ~ 72 h for both PH-HG designs.

3. Methods

3.1. Nuclear magnetic resonance spectroscopy

^1H and ^{13}C NMR spectroscopy was performed using a Bruker Ultrashield 400 MHz (100 MHz for ^{13}C NMR) instrument and the data were processed using Mestre Nova 14.3 software.[61].

3.2. Total porosity, swelling ratio, gel fraction calculations

Total porosity calculations and density measurements were obtained from dried polyHIPE samples using a home-built Archimedes balance from three replicates following protocols previously established in our lab.[47,48,60] We calculated the total porosity of the PHs using Eq. (1) where ρ is the average density of the bulk PDMS (0.975 g/mL), ρ^* is the measured density of individual polyHIPE samples (Table S1), and Φ is total porosity.

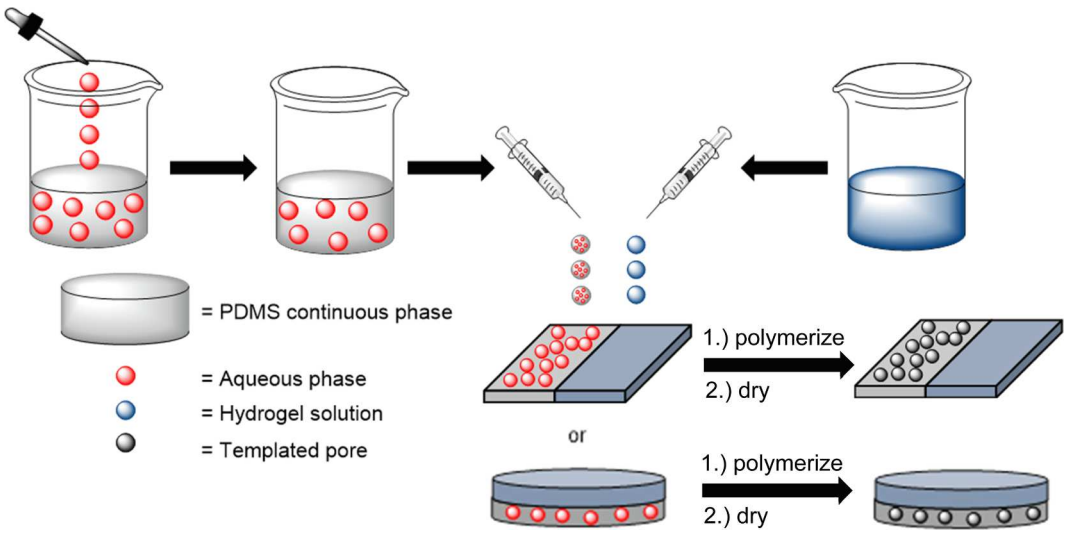

Fig. 1. Overview of horizontal-polyHIPE-hydrogel or stacked-polyHIPE-hydrogel synthesis by patterning an emulsion with a hydrogel solution. Emulsion **(red/grey)** can be patterned with a hydrogel **(blue)** to produce a polyHIPE-hydrogel composite after polymerization and drying.

$$\Phi(\%) = (1 - \frac{\rho^*}{\rho}) \times 100 \quad (1)$$

Swelling ratio and gel fraction were obtained after purification of hydrogels. Gel fraction and swelling ratios were calculated using three replicates. The prepared organogels were first solvent exchanged to deionized water for 72 h with water changes every 12 h. They were then dried in a vacuum oven for 48 h and reswollen for 48 h to determine the swelling ratio. After recording the mass of the swollen gel (M_s), the hydrogels were again dried in the vacuum oven for 48 h and the dry mass measured (M_d) (Table S2). The swelling ratio was calculated according to Eq. (2) as previously described[61]:

$$SwellingRatio(\%) = \frac{M_s - M_d}{M_d} \times 100 \quad (2)$$

Gel fractions of the hydrogels were calculated using Eq. (3) where M_i is the initial mass of polymers in the hydrogel (Table S2) as previously described [61].

$$GelFraction(\%) = \frac{M_d}{M_i} \times 100 \quad (3)$$

3.3. Scanning electron microscopy imaging and average pore diameter measurements

Average pore morphology observations were obtained by analysis of scanning electron microscopy (SEM) images using a Scanning Electron Microscope (Low-Vac) (FEI XL-30) equipped with an EDAX detector. [47,48,60] Cross sections of the materials were cut from dried polyHIPEs or composites from chosen locations and fixed onto aluminum stubs and imaged at an accelerating voltage of 15 kV. Average pore diameters were obtained from analysis of SEM images using ImageJ software by measuring 100 pores from SEM images for each formulation.

3.4. Oscillatory frequency and compression rheology characterization

Mechanical characterization was performed and adapted following protocols established for similar materials in our lab.[47,48,60] Viscoelastic properties of all prepared materials were obtained using rheology analysis by performing oscillatory frequency sweeps (0.1–100 Hz; 0.1% strain, 22 °C) with a Discovery Series Hybrid Rheometer (Model HR-2, TA Instruments) using 20 mm diameter parallel plates and controlled temperature using an advanced Peltier system on three replicate materials. Samples with a 20 mm diameter and a height of ~ 3 mm were used during rheological characterization that were obtained using a metal ring to punch out the sample. PolyHIPEs were characterized using rheology from samples dried for 48 h. Hydrogels were characterized using rheology from samples reswollen in deionized water for 48 h. For horizontally layered-PH-HG composites, the hydrogel section was first cut away from the polyHIPE using a scalpel, and both the hydrogel and polyHIPE were dried in a vacuum oven for 48 h. Both portions were then prepared and characterized using rheology the same way as non-layered samples. The metal ring was used to punch out 20 mm by 3 mm sized sections from either side of the interface (Fig. S3). Mechanical analysis was performed on dried polyHIPEs using compression testing (0.5 mm/min, 50 N maximum normal force, 22 °C) with a Discovery Series Hybrid Rheometer (Model HR-20, TA Instruments) using 20 mm diameter parallel plates on three replicates. The Young's Modulus was recorded as the slope of the initial linear portion of the stress–strain curve (strain < 2%) and the maximum strain for each formulation is recorded as the point in which the axial force reaches 50 N (stress = ~ 160 kPa) while compressing the material as this is the maximum for the instrument. Samples were prepared by cutting out 20 mm diameter disks with a height of ~ 3 mm using a metal ring as a punch following the same locations as described for rheological analysis.

4. Results and discussion

4.1. Synthesis and physical properties of non-layered polyHIPEs and hydrogels

We first prepared individual PDMS-based polyHIPEs and hydrogels as controls for the composite materials. We chose to keep the volume fraction of dispersed phase in the HIPEs constant at 70%, as this formulation has a high enough yield stress to maintain its shape during patterning with the hydrogel precursor solution and provides a highly porous polyHIPE following curing. Scheme 1 shows the thiol-ene crosslinking reaction between the pendent thiolated-PDMS and telechelic vinyl-PDMS in the continuous phase of the emulsion to prepare the polyHIPEs.

We tested thiol to ene ratios of 1:2, 1:1, and 2:1 (thiol:ene) and named the polyHIPEs by the naming system $PH_{T:E}$ where "T" is the thiol content and "E" is the alkene content. For example, sample $PH_{1:1}$ is a polyHIPE with a thiol to ene ratio of 1:1. We chose these stoichiometric ratios based on our previous work where we found that the ratio of thiol to ene had a significant impact on the storage modulus of PDMS polyHIPEs under dynamic mechanical analysis experiments.[47,48] In that work, polyHIPEs with a total porosity of ~ 40% were prepared, much lower than the total porosity of the materials prepared here.

We characterized the polyHIPEs using SEM, and the SEM images of the dried polyHIPEs are shown in Fig. 2**.**

The SEM images show interconnected pores for $PH_{1:1}$ and $PH_{2:1}$ (Fig. 2**b and 2c** respectively), where both images appear qualitatively similar with respect to the pore morphology and pore interconnectivity. For $PH_{1:1}$ and $PH_{2:1}$, spherical pores are observed, and the pores have an average diameter of 18 ± 9 μm and 17 ± 8 μm respectively from analysis of the SEM images using ImageJ software. In contrast, $PH_{1:2}$, with an excess amount of alkene-containing PDMS, does not show a porous structure (Fig. 2**a**). This type of morphology is indicative of a collapsed pore structure that can occur when using soft, low T_g, polymers as observed in similar PDMS-based porous monoliths[62] as well as our previous work where polyHIPEs with a volume fraction of dispersed phase of 80% experienced pore collapse.[60] The $PH_{1:2}$ materials were partially optically transparent with appreciable volume loss, further confirming the non-porous crosslinked PDMS, while $PH_{1:1}$ and $PH_{2:1}$ maintained the expected white monolith appearance with negligible volume loss (Fig. S4).

We characterized total porosity of the polyHIPEs, and the results are presented in Table 1**.**

We obtained the expected porosity of ~ 70% for the polyHIPE with a 1:1 thiol to ene ratio ($PH_{1:1}$), where the initial volume of dispersed phase resulted in the expected total porosity. However, for the off-stoichiometric ratios, this templating effect is not observed. A lower Φ_{exp} of 56% was seen for $PH_{2:1}$, and for $PH_{1:2}$ a very low value for Φ_{exp} of 2% was determined. The observed decrease in total porosity for $PH_{2:1}$ and $PH_{1:2}$ is a result of pore collapse during the drying process. Therefore, highly porous PDMS monoliths can only be prepared using formulations $PH_{1:1}$ and $PH_{2:1}$.

We designed the hydrogels prepared in this work to have a compatible polymerization with the polyHIPEs to promote covalent bonding between the layers. For this reason, we prepared PEG/PDMS hydrogels as outlined in Scheme 2 using UV-initiated thiol-ene click reactions between acrylate-terminated PEG and the thiolated-PDMS used in the polyHIPEs. The crosslinking occurred in a mixture of THF/MeOH, as the PDMS-thiol is insoluble in water. The resulting organogels were immediately solvent exchanged to water to give the hydrogels.

We chose to prepare hydrogels with solid contents of 5 wt% or 10 wt % to target different swelling ratios and viscoelastic properties in the hydrogels. The thiol to ene ratio of all hydrogel formulations was held constant at a 1:1 (thiol:ene) ratio. We named the hydrogels according to the solid contents of the precursor solutions as $HG_{X\%}$ where "X" is the solid content. For example, $HG_{10\%}$ is a hydrogel prepared with an initial

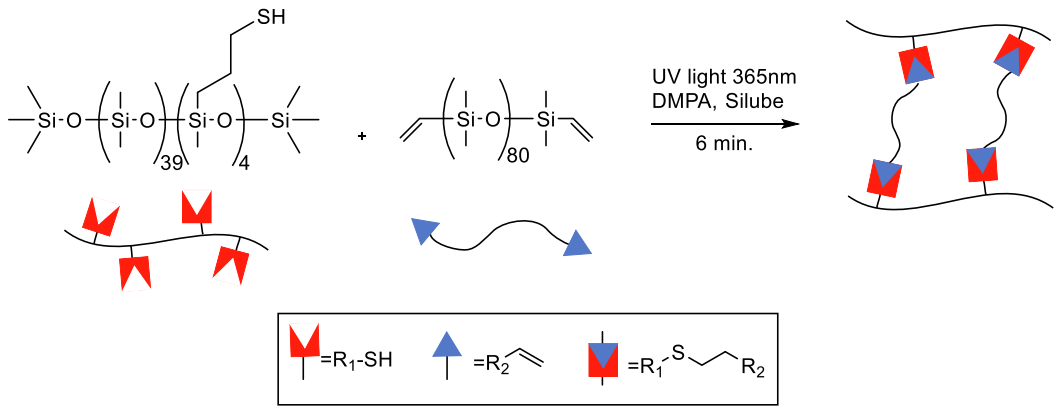

Scheme 1. Crosslinking reaction occurring in the continuous phase between pendent thiolated-PDMS and vinyl terminated-PDMS.

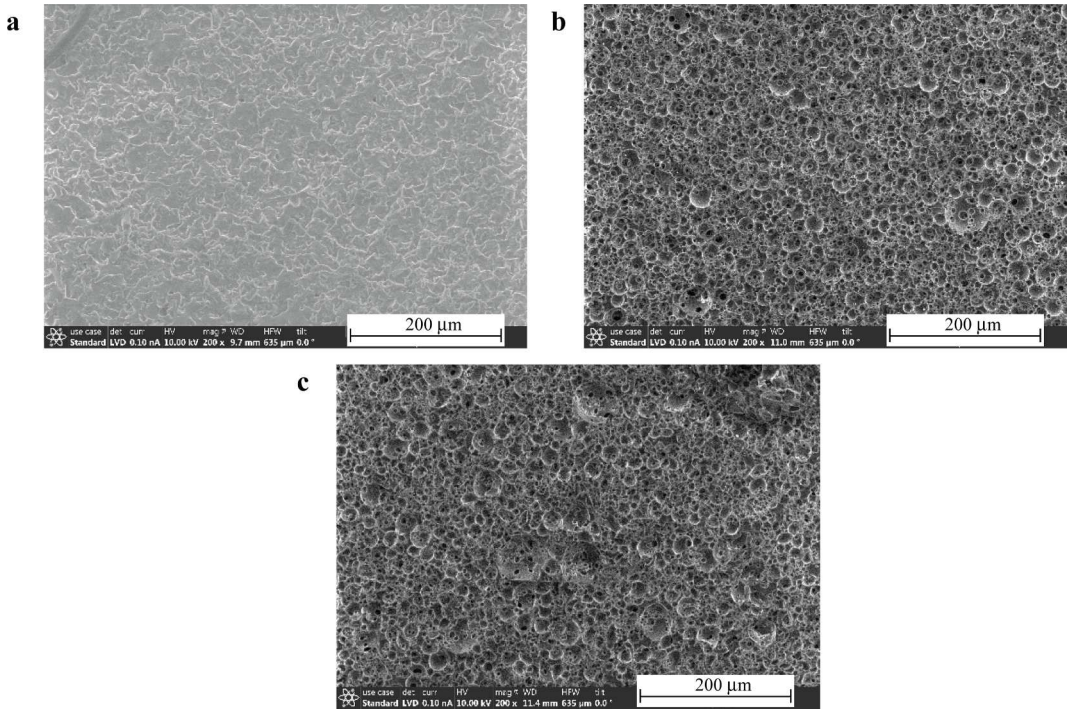

Fig. 2. SEM images of cross sections of dried polyHIPEs with varied thiol to ene ratios. **(a)** $PH_{1:2}$, **(b)** $PH_{1:1}$ and **(c)** $PH_{2:1}$. Scale bar is 200 µm for images.

Table 1
Total porosity results and average pore diameter of PHs with varied thiol to ene ratios **($PH_{1:2}$ – $PH_{2:1}$),** swelling ratio, and gel fraction results of HGs with varied theoretical solid content **($HG_{5\%}$ – $HG_{10\%}$).**

Material	Experimental Total Porosity[a] Φ_{exp} (%)	Pore Diameter (µm)	Swelling Ratio[b] (%)	Gel Fraction[c] (%)
$PH_{1:2}$	2 ± 1%	–	–	–
$PH_{1:1}$	67 ± 2%	18 ± 9	–	–
$PH_{2:1}$	56 ± 2%	17 ± 8	–	–
$HG_{5\%}$	–	–	680 ± 28%	89 ± 4%
$HG_{10\%}$	–	–	550 ± 16%	93 ± 2%

[a] Calculated from Eq. (1).
[b] Calculated from Eq. (2).
[c] Calculated from Eq. (3).

total solids content of 10 wt%. The as-prepared organogels were solvent exchanged to deionized water, dried, and reswollen in deionized water to obtain the swelling ratio and gel fraction, and these results are present in Table 1. When comparing the swelling ratios, $HG_{5\%}$ possessed a swelling ratio of ~ 700% and $HG_{10\%}$ had a swelling ratio of ~ 550%.

4.2. Porosity, swelling ratio, and gel fraction of H-PH-HG composites

Having characterized the single-component materials, we prepared horizontally-layered polyHIPE-hydrogel (H-PH-HG) composite materials. We prepared two series of H-PH-HGs to investigate if the process of layering a polyHIPE with a hydrogel impacts the total porosity or pore morphology of the polyHIPEs or the swelling of the hydrogels. In the first series, we held the solid content of the hydrogel layer constant at 10 wt% and changed the thiol to ene ratio in the polyHIPE layer to either a 1:1 or 2:1 ratio to selectively tune the polyHIPE properties. In the second series we held the thiol to ene ratio of the polyHIPE constant at a 1:1 ratio and changed the hydrogel solids content to 5 wt% or 10 wt%. We named the layered composites according to the formulation of both the polyHIPE and hydrogel. For example, H-$PH_{1:1}$-$HG_{10\%}$ was prepared from a polyHIPE with a thiol to ene ratio of 1:1 with a hydrogel having a solid content of 10 wt%. The composite materials were prepared,

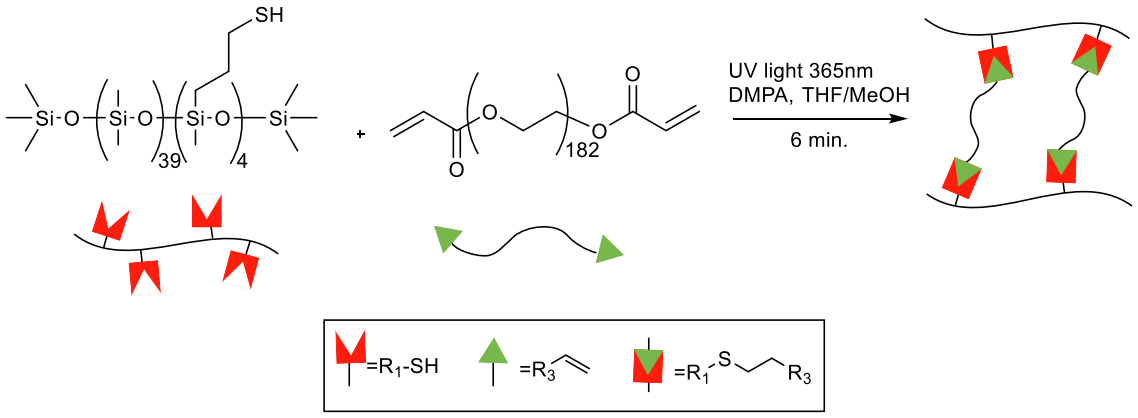

Scheme 2. Crosslinking reaction to form the hydrogel network between pendent thiolated-PDMS and PEG-diacrylate.

purified, and characterized in the same manner as the single-component materials and the results are presented in Table 2 and Fig. 3.

We chose not to prepare composites using the $PH_{1:2}$ formulation due to the pore collapse observed in the non-layered polyHIPEs. Furthermore, we observed that materials prepared with $HG_{5\%}$ were too weak to maintain a strong interface with the polyHIPE and the hydrogel delaminated from the polyHIPE. The results in Table 2 compared to Table 1 show that there was no significant difference in the properties of the composite materials from the single-component polyHIPEs or hydrogels regarding total porosity, swelling ratio, and gel fraction for composites prepared with 10 wt% hydrogels. SEM and digital images (Fig. 3) show a well-defined interface between the polyHIPE and hydrogel components of the layered composites. These images are representative of both formulations tested.

Optical images **(**Fig. 3**a and 3b)** show a defined interface is maintained after solvent exchange to water **(**Fig. 3**a)** and after drying **(**Fig. 3**b)**. SEM images **(**Fig. 3**c and 3d)** show a more detailed picture of the interface. The interconnected-spherical porous structure corresponding to the polyHIPE **(yellow arrow in** Fig. 3**c)** is observed and not disturbed from the layering process. We observe a dispersity in pore sizes with both H-$PH_{1:1}$-$HG_{10\%}$ and H-$PH_{2:1}$-$HG_{10\%}$ obtaining an average pore diameter of ~ 18 μm, and compared to the non-layered controls, there was no difference in average pore diameter. There is no visual delamination of the hydrogel from the polyHIPE, even during the significant volume changes of the hydrogel that occurs during drying. The hydrogel did experience a distortion upon drying and after reswelling in some samples, resulting in a non-uniform shape of the hydrogel. An example is shown from a sample of H-$PH_{1:1}$-$HG_{10\%}$ in Fig. S5. This behavior is presumably due to the hydrogel being restricted along the side where it is bonded to the polyHIPE, resulting in a non-uniform shape during drying. Both formulations could undergo purification, drying, and reswelling processes without significant delamination, showing that this technique can be used to prepare layered polyHIPE-hydrogel composites with robust interfaces in a simple and rapid manner.

Table 2
PolyHIPE experimental porosity, average pore diameter, hydrogel swelling ratio, and gel fraction results of layered composites **(H-$PH_{1:1}$-$HG_{10\%}$ and H-$PH_{2:1}$-$HG_{10\%}$).**

Material	Experimental Total Porosity[a] Φ_{exp} (%)	Pore Diameter (μm)	Swelling Ratio[b] (%)	Gel Fraction[c] (%)
H-$PH_{1:1}$-$HG_{10\%}$	61 ± 2%	19 ± 8	540 ± 33%	83 ± 5%
H-$PH_{2:1}$-$HG_{10\%}$	55 ± 3%	15 ± 7	510 ± 6%	91 ± 2%

[a] Calculated from Eq. (1).
[b] Calculated from Eq. (2).
[c] Calculated from Eq. (3).

4.3. Mechanical analysis of H-PH-HG composites

The H-PH-HGs composites were further characterized using rheology and compared to the polyHIPE and hydrogel controls to determine if there were any difference in storage (G') and loss (G'') moduli between the single component and composite materials **(**Fig. 4**)**. Rheological analysis was performed on portions cut using a metal punch from either side of the H-PH-HG interface (Fig. S3) and compared to the single component materials. The polyHIPEs (both PHs and H-PHs) are characterized in the dried state and the hydrogels (both HGs and H-HGs) are characterized in the swollen state. The sections cut from H-PH-HGs are denoted by which side they are cut from. For example, in the composite H-$PH_{1:1}$-$HG_{10\%}$, the portions cut from the polyHIPE side of a composite are described as H-$PH_{1:1\text{-}10\%}$ and the hydrogel side is H-$HG_{10\%\text{-}1:1}$ in Fig. 4a. The hydrogel solid content was constant at 10 wt% when the thiol to ene ratio in the polyHIPE was varied (Fig. 4).

We observed no significant changes in the storage moduli for the polyHIPE and hydrogel portions of horizontal composites compared to the controls for either polyHIPE formulation. Specifically, for polyHIPEs with a 1:1 thiol to ene ratio ($PH_{1:1}$ and H-$PH_{1:1\text{-}10\%}$) the control and the composite both obtained G' values of ~ 35 kPa (filled black bar and filled red bar in Fig. 4**a**). Furthermore, the control hydrogel ($HG_{10\%}$) and the hydrogel portion of the composite (H-$HG_{10\%\text{-}1:1}$) obtained G' values of 43 ± 9.3 kPa and 44 ± 4.8 kPa respectively. We observed similar behavior for horizontally layered PH-HG composites prepared from polyHIPEs having a thiol to ene ratio of 2:1. For example, $PH_{2:1}$ and H-$PH_{2:1\text{-}10\%}$ had G' values of 36 ± 3.4 kPa and 34 ± 3.5 kPa respectively. Additionally, the hydrogel portion of the composite (H-$HG_{10\%\text{-}2:1}$) was similar to the control ($HG_{10\%}$) having a G' value of 34 ± 5.3 kPa (Fig. 4). Importantly, we did not observe any differences in the storage moduli of the hydrogel from either composite (H-$HG_{10\%\text{-}1:1}$ compared to H-$HG_{10\%\text{-}2:1}$), indicating the polyHIPE formulation did not impact the G' of the hydrogel. Unexpectedly, changing the thiol to ene ratio in the polyHIPE formulation resulted in no change in the storage moduli of the polyHIPEs, and all the polyHIPEs tested obtained G' values of ~ 36 kPa under shear. We expected polyHIPEs with an equal thiol to ene ratio (1:1) to have a higher storage modulus than polyHIPEs with an unbalanced stoichiometry based on our previous results.[47,48] In our previous studies, we prepared polyHIPEs with lower porosity (40%) and we observed that changing the thiol to ene ratio from 1:1 to 2:1 resulted in polyHIPEs with a significantly lower storage modulus under tension. [47] We hypothesized that the thiol to ene ratio had a smaller impact on the storage shear modulus in the current study as these higher porosity materials are much softer. To test this hypothesis, the polyHIPEs were furthered characterized using compressive measurements. The results

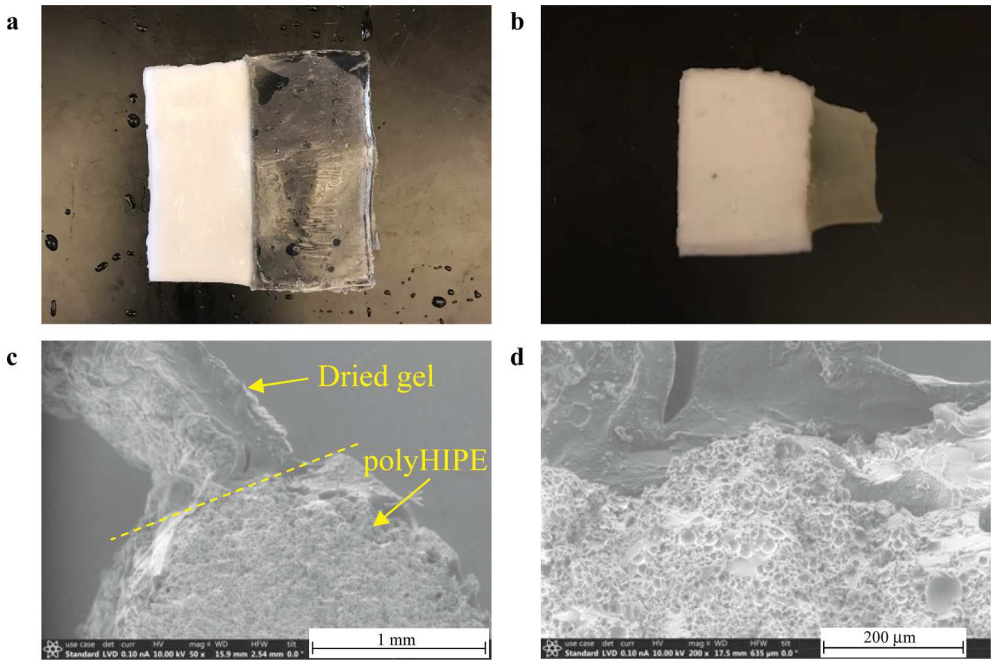

Fig. 3. Digital **(top)** and SEM **(bottom)** images of H-$PH_{1:1}$-$HG_{10\%}$. The white portion in digital images corresponds to the polyHIPE portion while the clear portion is the hydrogel. Image **(a)** is the composite after purification and **(b)** is after drying. SEM images are of cross sections from the interface of the composite after drying where the yellow dashed line in image **(c)** is highlighting the exact interface between the polyHIPE and hydrogel portions and **(d)** is under higher magnification at the interface. Scale bar is 1 mm for image **(c)** and 200 µm for image **(d)**.

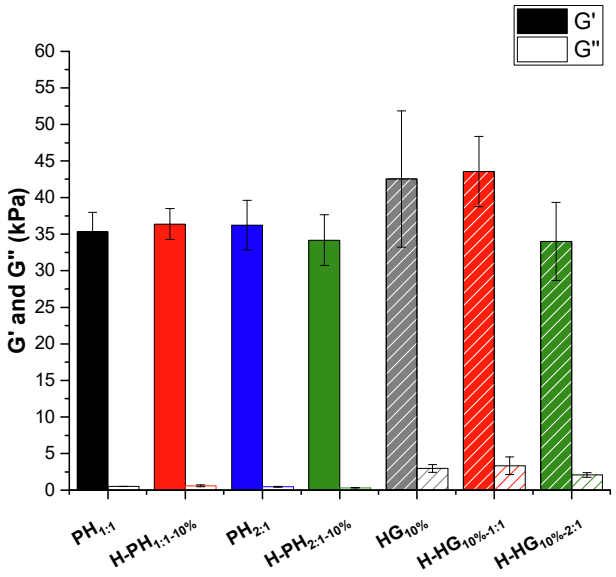

Fig. 4. Storage and loss moduli oscillation frequency sweep rheology plots at 10 Hz of dried polyHIPEs, hydrogels, and H-PH-HG composites where the polyHIPE formulation was varied. PolyHIPEs are represented by filled and open bars and hydrogels correspond to striped-filled and stripped-open bars for G' and G'' respectively. Each entry is plotted as an average of three replicates.

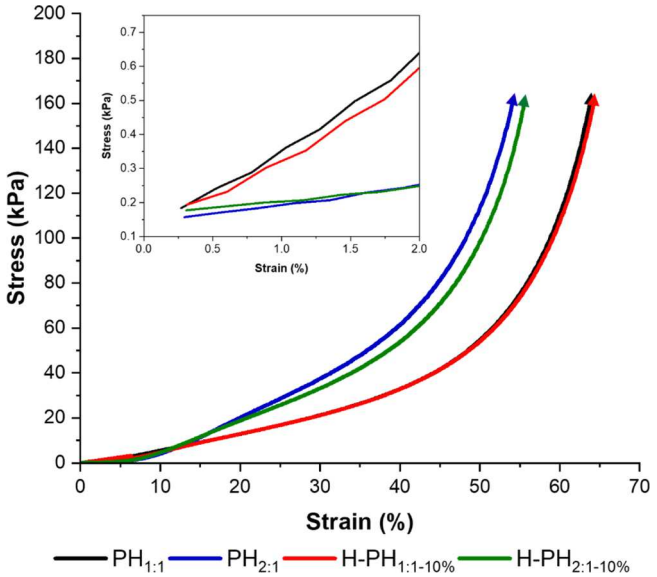

Fig. 5. Compressive stress–strain plot for control and composite dry polyHIPEs. The inset plot highlights the initial linear portion of each sample at low strain used to calculate the Young's Modulus for each sample. This plot corresponds to one sample at each formulation and is indicative of the trends observed for all samples. The arrow on each line indicates the samples did not fail during the compression test.

from one set of materials are presented in Fig. 5, and the remaining data are in Fig. S7.

The polyHIPEs recovered their original height after compression with no observable visual deformations for all the samples tested.The compressive stress–strain curves show a difference in the maximum strain (ε_{max}) (Fig. 5) and Young's Modulus (E) (inset plot in Fig. 5) between polyHIPEs where the thiol to ene ratio is either 1:1 or 2:1. For the $PH_{1:1}$ control we observed a Young's Modulus value of 25 ± 2.0 kPa and an ε_{max} of ~ 64%, while $PH_{2:1}$ obtained a Young's Modulus value of 7.1 ± 1.0 kPa and an ε_{max} of ~ 54%. Furthermore, the densification point occurs at a higher strain for $PH_{1:1}$ indicated by an increase in the slope of the line at ~ 40% compared to $PH_{2:1}$ where the densification point occurs ~ 30%. The densification point in air-filled polymer foams can be used to describe the point at which enough force has been applied to the material to collapse the pore structure and the material begins to act as a solid polymeric monolith.[63] Collectively, these results suggest that $PH_{2:1}$ is a weaker polymer network than $PH_{1:1}$. Similar results were observed for the horizontal composites, where H-$PH_{1:1\text{-}10\%}$ obtained a Young's Modulus value of 20 ± 4.4 kPa and H-$PH_{2:1\text{-}10\%}$ obtained a lower Young's Modulus value of 5.8 ± 2.8 kPa (red line vs. green line in Fig. 5). In summary, the layering process has negligible effects on the resulting properties of each component of the composite, with respect to porosity and pore morphology, swelling ratio, gel fraction, and

mechanical properties (G', E, and ε_{max}). Therefore, the properties of both the hydrogel and polyHIPE can be independently tuned and studied by choosing the formulations of the single-component materials before composite materials are prepared, simplifying the process of designing and preparing the layered systems for their applications. Furthermore, for the hydrogel and polyHIPE components tested in this work, we obtained G' values that are comparable to human tissue including skeletal muscle and tendon of ~ 15–30 kPa and ~ 20–40 kPa respectively, making these composites potential candidates for biomaterial applications.[64,65] The pore sizes observed in the polyHIPE portion in the composites range from ~ 10–150 μm and show high interconnectivity, which is comparable to other polyHIPEs used as tissue engineering scaffolds.[51].

4.4. Preparation of S-PH-HGs

Having prepared and characterized horizontally layered composites, polyHIPEs and hydrogels were patterned vertically to produce *stacked*-polyHIPE-hydrogel composites (S-PH-HGs) and explore the layering process in a different geometry. Digital images of hydrated and dry materials are presented in Fig. 6.

Stacked composites were prepared using the same formulations as the horizontal composites. The stacked composite prepared using a hydrogel with 5 wt% solids were too weak for handling, as observed in the horizontal composites. We observed significant delamination of the hydrogel and the polyHIPE layers after drying for all formulations tested in these materials (Fig. S6). A similar result is seen in related work from Okay and coworkers[66] where it was shown that a large mismatch in swelling ratios between layered hydrogels caused the interface between layers to tear and fail. The large mismatch in swelling observed in our work between the hydrogel and polyHIPE could result in bond rupture at the interface of the stacked hydrogels. We hypothesize that this is observed in vertically-stacked composites rather than horizontally-layered composites due to the greater surface area of the interfacial region for stacked-composites. This larger interfacial region appears to experience a larger deformation compared to horizontal patterns (Fig. 6**a** compared to Fig. 3**a**) that results in bond rupture between layers in the stacked patterns. Further materials characterization of the vertically-stacked composites was not performed due to the interfacial delamination.

4.5. Digital images of multi-layered H-PH-HGs

We have extended the results of the horizontally-layered composites by preparing *multi*-layered horizontal composites using the $PH_{1:1}$-$HG_{10\%}$ formulation to demonstrate the capabilities of our patterning method (Fig. 7**)**.

A five-layer design was first prepared, and it was observed to exhibit the same swelling profiles as the two-layer designs. The hydrogel layer expanded after being placed in water, and the differences in size can be observed when comparing the dry state to the hydrated state (Fig. 7**a and 7b** respectively). We observed no delamination between the layers and a maximum swollen state was achieved in ~ 2 h. The same horizontal patterning technique was used to prepare an alternating polyHIPE-hydrogel composite with seven horizontal layers (Fig. 7**c and d**). Again, the hydrogel layer expanded after being submerged in water without delaminating from the polyHIPE layers. Even in multiple alternating layers of polyHIPE and hydrogel components, there was no observable interlayer mixing, and a clear and defined interface was maintained upon preparation, purification, and reswelling for all horizontal patterning and minimal, if any, delamination occurs for horizontally patterned composites after reswelling. We envision that different polyHIPEs can be patterned with the hydrogel in this platform, and further, that these materials can be translated across other related areas for the synthesis of novel tunable composite materials with well-defined interfaces.

5. Conclusions

We have prepared horizontally-layered and vertically-stacked polyHIPE-hydrogel composite materials with well-defined interfaces that show negligible inter-layer mixing. The physical and mechanical properties of the materials in the composite materials (H-PH-HGs) matched the corresponding single-material controls. Specifically, hydrogels prepared from layered- and non-layered protocols obtained swelling ratios and gel fractions of ~ 500 % and 85% respectively, and the hydrogels obtained G' values of ~ 35 kPa. The mechanical properties of polyHIPEs, layered and non-layered, could be controlled by varying the thiol-ene ratio with polyHIPEs prepared from a 1:1 ratio obtained the highest Youngs Modulus of ~ 25 kPa and maximum strain of 65% compared to polyHIPEs having a 2:1 ratio that obtained values of ~ 7 kPa and 55% respectively. The layered and non-layered polyHIPEs both obtained an interconnected open-cell porosity with pore sizes having an average diameter of ~ 18 μm and a total porosity of ~ 65% for polyHIPEs prepared from a 1:1 thio-ene ratio. These results support our hypothesis that using photoinitiated crosslinking reactions between complementary thiol- and ene- functionalized polymers result in composite materials with defined interfaces between hydrogel and porous polyHIPE layers. As a result of this work, we have introduced a new technique to prepare layered-composites with spatially controlled polyHIPE and hydrogel layers. Previous literature reported the preparation and characterization of layered polyHIPEs [6,59] or layered hydrogels [56,58], but, to our knowledge, materials have not previously been prepared that combine the advantageous properties of both polyHIPEs *and* hydrogels in spatially defined materials as we have demonstrated here. Furthermore, our synthesis method is a simple and easily adaptable technique that does not require complex instruments or reagents and results in materials with controllable physical and mechanical properties. We envision this work providing a robust platform for preparing polyHIPE-hydrogel composite materials, and future work may focus on introducing functionality to the polyHIPE and hydrogel networks while maintaining defined interfaces for applications including biomaterials

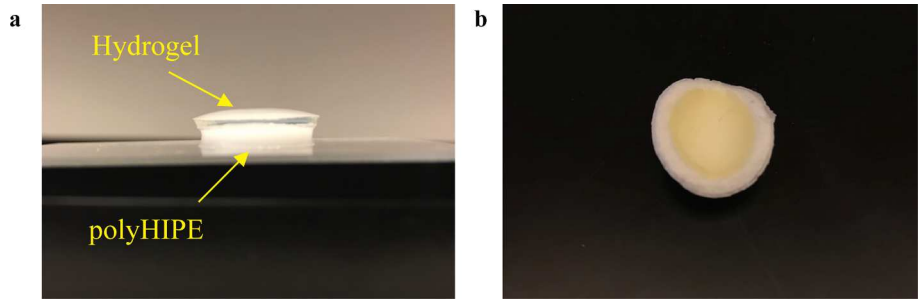

Fig. 6. Digital images of S-$PH_{1:1}$-$HG_{10\%}$. Image **(a)** is the composite after solvent exchange to water and **(b)** is a top view of the composite after drying. The white portion in digital images corresponds to the polyHIPE portion while the clear or yellow portion is the hydrogel (**yellow arrows in a**).

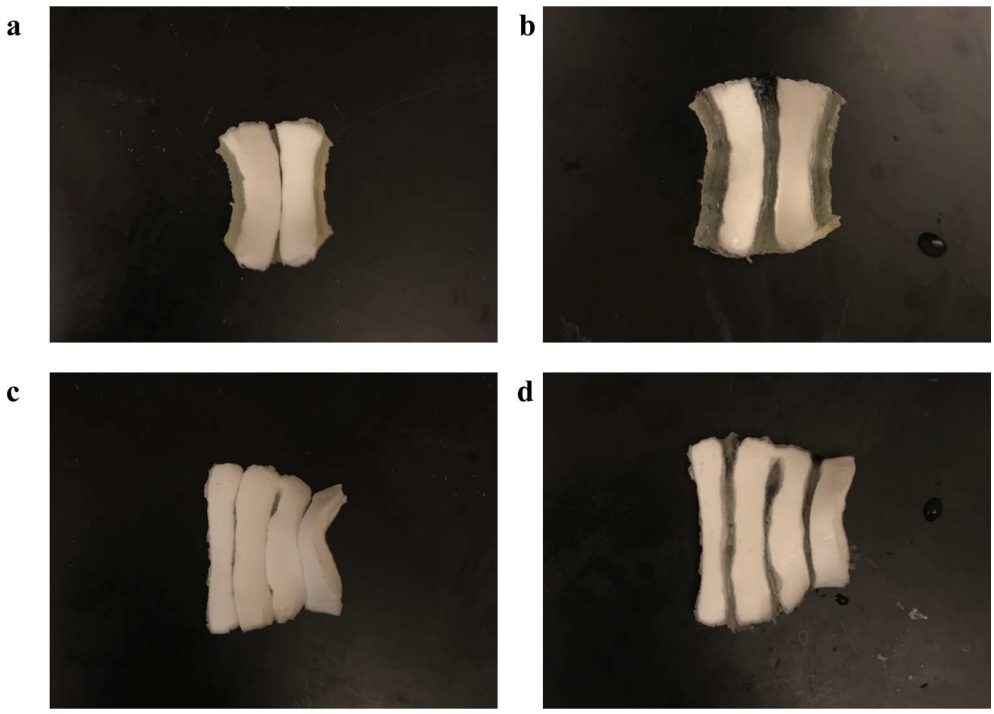

Fig. 7. Digital images of five-layered composite (**a and b**) and seven-layered composite (**c and d**) in the dried (**left**) and hydrated (**right**) state. The polyHIPE portion is white and the hydrogel portion is clear in each composite.

or soft robotics.

CRediT authorship contribution statement

Tucker J. McKenzie: Methodology, Investigation, Writing – original draft. **Christian Cawood:** Investigation. **Chelsea Davis:** Investigation. **Neil Ayres:** Conceptualization, Writing – original draft, Writing – review & editing, Supervision, Project administration, Funding acquisition.

Declaration of Competing Interest

The authors declare the following financial interests/personal relationships which may be considered as potential competing interests: Neil Ayres reports financial support was provided by National Science Foundation.

Data availability

Data will be made available on request.

Acknowledgements

We thank the National Science Foundation (DMR-1940518) for the resources to conduct this work. We also thank Dr. Spencer Hendrickson and Prof. Ryan White for help with 3D printing of the templates used in this work. We thank Dr. Melodie Fickenscher for help with SEM imaging and use of the HR-20 rheometer.

Appendix A. Supplementary material

Supplementary data to this article can be found online at https://doi.org/10.1016/j.jcis.2023.04.132. Additional information can be found on the techniques and characterization of materials presented in this manuscript such as ^{1}H and ^{13}C NMR spectra of PEG-DA; images of the patterning methods; sample preparation for rheology characterization; and density measurements for total porosity calculations

References

[1] A. Di Luca, A. Longoni, G. Criscenti, C. Mota, C. Van Blitterswijk, L. Moroni, Toward mimicking the bone structure: Design of novel hierarchical scaffolds with a tailored radial porosity gradient, Biofabrication. 8 (2016) 1–15, https://doi.org/10.1088/1758-5090/8/4/045007.

[2] L. Sardelli, D.P. Pacheco, L. Zorzetto, C. Rinoldi, W. Święszkowski, P. Petrini, Engineering biological gradients, J Appl Biomater Funct Mater. 17 (2019). Doi: 10.1177/2280800019829023.

[3] X. Li, R. Cheng, Z. Sun, W. Su, G. Pan, S. Zhao, J. Zhao, W. Cui, Flexible bipolar nanofibrous membranes for improving gradient microstructure in tendon-to-bone healing, Acta Biomater. 61 (2017) 204–216, https://doi.org/10.1016/j.actbio.2017.07.044.

[4] A. Marrella, M. Aiello, R. Quarto, S. Scaglione, Chemical and morphological gradient scaffolds to mimic hierarchically complex tissues: From theoretical modeling to their fabrication, Biotechnol Bioeng. 113 (2016) 2286–2297, https://doi.org/10.1002/bit.25994.

[5] X. Hu, W. Li, L. Li, Y. Lu, Y. Wang, R. Parungao, S. Zheng, T. Liu, Y. Nie, H. Wang, K. Song, A biomimetic cartilage gradient hybrid scaffold for functional tissue engineering of cartilage, Tissue Cell. 58 (2019) 84–92, https://doi.org/10.1016/j.tice.2019.05.001.

[6] S. Jurjevec, E. Žagar, S. Kovačič, Functional macroporous amphoteric polyelectrolyte monoliths with tunable structures and properties through emulsion-templated synthesis, J Colloid Interface Sci. 575 (2020) 480–488, https://doi.org/10.1016/j.jcis.2020.05.016.

[7] S.C. Hess, A.X. Kohll, R.A. Raso, C.M. Schumacher, R.N. Grass, W.J. Stark, Template-particle stabilized bicontinuous emulsion yielding controlled assembly of hierarchical high-flux filtration membranes, ACS Appl Mater Interfaces. 7 (2015) 611–617, https://doi.org/10.1021/am506737n.

[8] F. Connolly, C.J. Walsh, K. Bertoldi, Automatic design of fiber-reinforced soft actuators for trajectory matching, Proc Natl Acad Sci USA. 114 (2017) 51–56, https://doi.org/10.1073/pnas.1615140114.

[9] G. Shimoga, D.S. Choi, S.Y. Kim, Bio-inspired soft robotics: Tunable photo-actuation behavior of azo chromophore containing liquid crystalline elastomers, Appl. Sci. (Switzerland). 11 (2021) 1–18, https://doi.org/10.3390/app11031233.

[10] K. Tian, J. Bae, S.E. Bakarich, C. Yang, R.D. Gately, G.M. Spinks, M. in het Panhuis, Z. Suo, J.J. Vlassak, 3D Printing of Transparent and Conductive Heterogeneous Hydrogel-Elastomer Systems, Adv. Mater. 29 (10) (2017) 1604827.

[11] D. Zhalmuratova, H.J. Chung, Reinforced Gels and Elastomers for Biomedical and Soft Robotics Applications, ACS Appl Polym Mater. 2 (2020) 1073–1091, https://doi.org/10.1021/acsapm.9b01078.

[12] A. Cheng, Z. Schwartz, A. Kahn, X. Li, Z. Shao, M. Sun, Y. Ao, B.D. Boyan, H. Chen, Advances in Porous Scaffold Design for Bone and Cartilage Tissue Engineering and Regeneration, Tissue Eng Part B Rev. 25 (2019) 14–29, https://doi.org/10.1089/ten.teb.2018.0119.

[13] B.S. Kim, E.J. Kim, J.S. Choi, J.H. Jeong, C.H. Jo, Y.W. Cho, Human collagen-based multilayer scaffolds for tendon-to-bone interface tissue engineering, J Biomed Mater Res A. 102 (2014) 4044–4054, https://doi.org/10.1002/jbm.a.35057.
[14] Y. Zheng, Q. Han, D. Li, F. Sheng, Z. Song, J. Wang, Promotion of tendon growth into implant through pore-size design of a Ti-6Al-4 V porous scaffold prepared by 3D printing, Mater Des. 197 (2021), 109219, https://doi.org/10.1016/j.matdes.2020.109219.
[15] Q. Chen, Q. Gao, X. Wang, D.W. Schubert, X. Liu, Flexible, conductive, and anisotropic thermoplastic polyurethane/polydopamine /MXene foam for piezoresistive sensors and motion monitoring, Compos Part A Appl Sci Manuf. 155 (2022), 106838, https://doi.org/10.1016/j.compositesa.2022.106838.
[16] Z. Ma, A. Wei, J. Ma, L. Shao, H. Jiang, D. Dong, Z. Ji, Q. Wang, S. Kang, Lightweight, compressible and electrically conductive polyurethane sponges coated with synergistic multiwalled carbon nanotubes and graphene for piezoresistive sensors, Nanoscale. 10 (2018) 7116–7126, https://doi.org/10.1039/c8nr00004b.
[17] S. Kovačič, M.S. Silverstein, Superabsorbent, High Porosity, PAMPS-Based Hydrogels through Emulsion Templating, Macromol Rapid Commun. 37 (2016) 1814–1819, https://doi.org/10.1002/marc.201600249.
[18] C. Nam, H. Li, G. Zhang, L.R. Lutz, B. Nazari, R.H. Colby, T.C.M. Chung, Practical Oil Spill Recovery by a Combination of Polyolefin Absorbent and Mechanical Skimmer, ACS Sustain Chem Eng. 6 (2018) 12036–12045, https://doi.org/10.1021/acssuschemeng.8b02322.
[19] G. Demirci, M.J. Niedźwiedź, N. Kantor-Malujdy, M. El Fray, Elastomer-Hydrogel Systems: From Bio-Inspired Interfaces to Medical Applications, Polymers (Basel). 14 (2022) 1822, https://doi.org/10.3390/polym14091822.
[20] M.T. Frassica, C.J. Demott, E.M. Ramirez, M.A. Grunlan, Spatially Controlled Templated Hydrogels for Orthopedic Interfacial Tissue Regeneration, ACS Macro Lett. 9 (2020) 1740–1744, https://doi.org/10.1021/acsmacrolett.0c00712.
[21] N.A. Peppas, J.Z. Hilt, A. Khademhosseini, R. Langer, Hydrogels in biology and medicine: From molecular principles to bionanotechnology, Adv. Mater. 18 (2006) 1345–1360, https://doi.org/10.1002/adma.200501612.
[22] E.M. Ahmed, Hydrogel: Preparation, characterization, and applications: A review, J Adv Res. 6 (2015) 105–121, https://doi.org/10.1016/j.jare.2013.07.006.
[23] J. Zhao, H. Tong, A. Kirillova, W.J. Koshut, A. Malek, N.C. Brigham, M.L. Becker, K. Gall, B.J. Wiley, A Synthetic Hydrogel Composite with a Strength and Wear Resistance Greater than Cartilage, Adv Funct Mater. 32 (2022) 2205662, https://doi.org/10.1002/adfm.202205662.
[24] W. Wei, Y. Ma, X. Yao, W. Zhou, X. Wang, C. Li, J. Lin, Q. He, S. Leptihn, H. Ouyang, Advanced hydrogels for the repair of cartilage defects and regeneration, Bioact Mater. 6 (2021) 998–1011, https://doi.org/10.1016/j.bioactmat.2020.09.030.
[25] J.R. Capadona, K. Shanmuganathan, D.J. Tyler, S.J. Rowan, C. Weder, Stimuli-responsive polymer nanocomposites inspired by the sea cucumber dermis, Science 319 (2008) (1979) 1370–1374, https://doi.org/10.1126/science.1153307.
[26] I.C. Liao, F.T. Moutos, B.T. Estes, X. Zhao, F. Guilak, Composite three-dimensional woven scaffolds with interpenetrating network hydrogels to create functional synthetic articular cartilage, Adv Funct Mater. 23 (2013) 5833–5839, https://doi.org/10.1002/adfm.201300483.
[27] M. Hua, S. Wu, Y. Ma, Y. Zhao, Z. Chen, I. Frenkel, J. Strzalka, H. Zhou, X. Zhu, X. He, Strong tough hydrogels via the synergy of freeze-casting and salting out, Nature. 590 (2021) 594–599, https://doi.org/10.1038/s41586-021-03212-z.
[28] Y.J. No, S. Tarafder, B. Reischl, Y. Ramaswamy, C. Dunstan, O. Friedrich, C.H. Lee, H. Zreiqat, High-Strength Fiber-Reinforced Composite Hydrogel Scaffolds as Biosynthetic Tendon Graft Material, ACS Biomater Sci Eng. 6 (2020) 1887–1898, https://doi.org/10.1021/acsbiomaterials.9b01716.
[29] J. Cui, M.A. Lackey, A.E. Madkour, E.M. Saffer, D.M. Griffin, S.R. Bhatia, A. J. Crosby, G.N. Tew, Synthetically simple, highly resilient hydrogels, Biomacromolecules. 13 (2012) 584–588, https://doi.org/10.1021/bm300015s.
[30] J. Cui, M.A. Lackey, G.N. Tew, A.J. Crosby, Mechanical Properties of End-Linked PEG/PDMS Hydrogels, Macromolecules. 45 (15) (2012) 6104–6110.
[31] C. Bilici, S. Ide, O. Okay, Yielding Behavior of Tough Semicrystalline Hydrogels, Macromolecules. 50 (2017) 3647–3654, https://doi.org/10.1021/acs.macromol.7b00507.
[32] M.S. Silverstein, PolyHIPEs: Recent advances in emulsion-templated porous polymers, Prog Polym Sci. 38 (2014) 199–234, https://doi.org/10.1016/j.progpolymsci.2013.07.003.
[33] T. Zhang, R.A. Sanguramath, S. Israel, M.S. Silverstein, Emulsion Templating: Porous Polymers and beyond, Macromolecules. 52 (2019) 5445–5479, https://doi.org/10.1021/acs.macromol.8b02576.
[34] C. Stubenrauch, A. Menner, A. Bismarck, W. Drenckhan, Emulsion and Foam Templating—Promising Routes to Tailor-Made Porous Polymers, Angewandte Chemie - International Edition. 57 (2018) 10024–10032, https://doi.org/10.1002/anie.201801466.
[35] R. Foudazi, HIPEs to PolyHIPEs, React Funct Polym. 164 (2021), 104917, https://doi.org/10.1016/j.reactfunctpolym.2021.104917.
[36] S. Xie, F. Svec, J.M.J. Fréchet, Preparation of porous hydrophilic monoliths: Effect of the polymerization conditions on the porous properties of poly (acrylamide-co-N, N′-methylenebisacrylamide) monolithic rods, J Polym Sci A Polym Chem. 35 (1997) 1013–1021, https://doi.org/10.1002/(sici)1099-0518(19970430)35:6<1013::aid-pola4>3.3.co;2-7.
[37] S. Kovačič, N. Drašinac, A. Pintar, E. Žagar, Highly Porous Cationic Polyelectrolytes via Oil-in-Water Concentrated Emulsions: Synthesis and Adsorption Kinetic Study, Langmuir. 34 (2018) 10353–10362, https://doi.org/10.1021/acs.langmuir.8b01645.
[38] N.R. Cameron, A. Barbetta, The influence of porogen type on the porosity, surface area and morphology of poly(divinylbenzene) polyHIPE foams, J Mater Chem. 10 (2000) 2466–2471, https://doi.org/10.1039/B003596N.
[39] H.C. Kolb, M.G. Finn, K.B. Sharpless, Click Chemistry: Diverse Chemical Function from a Few Good Reactions, Angewandte Chemie - International Edition. 40 (2001) 2004–2021, https://doi.org/10.1002/1521-3773(20010601)40:11<2004::AID-ANIE2004>3.0.CO;2-5.
[40] R.K. Iha, K.L. Wooley, A.M. Nyström, D.J. Burke, M.J. Kade, C.J. Hawker, Applications of Orthogonal "Click" Chemistries in the Synthesis of Functional Soft Materials, Chem Rev. 109 (2009) 5620–5686, https://doi.org/10.1021/cr900138t.
[41] M.J. Kade, D.J. Burke, C.J. Hawker, The power of thiol-ene chemistry, J Polym Sci A Polym Chem. 48 (2010) 743–750, https://doi.org/10.1002/pola.23824.
[42] C.E. Hoyle, C.N. Bowman, Thiol-ene click chemistry, Angew. Chem. – Int. Ed. 49 (2010) 1540–1573, https://doi.org/10.1002/anie.200903924.
[43] A.B. Lowe, Thiol-ene "click" reactions and recent applications in polymer and materials synthesis: A first update, Polym Chem. 5 (2014) 4820–4870, https://doi.org/10.1039/c4py00339j.
[44] J.L. Ratcliffe, M. Walker, A.M. Eissa, S. Du, S.A. Przyborski, A.L. Laslett, N. R. Cameron, Optimized peptide functionalization of thiol-acrylate emulsion-templated porous polymers leads to expansion of human pluripotent stem cells in 3D culture, J Polym Sci A Polym Chem. 57 (2019) 1974–1981, https://doi.org/10.1002/pola.29353.
[45] B. Aldemir Dikici, A. Malayeri, C. Sherborne, S. Dikici, T. Paterson, L. Dew, P. Hatton, I. Ortega Asencio, S. MacNeil, C. Langford, N.R. Cameron, F. Claeyssens, Thiolene-and Polycaprolactone Methacrylate-Based Polymerized High Internal Phase Emulsion (PolyHIPE) Scaffolds for Tissue Engineering, Biomacromolecules. 23 (2022) 720–730, https://doi.org/10.1021/acs.biomac.1c01129.
[46] M.E. Whitely, J.L. Robinson, M.C. Stuebben, H.A. Pearce, M.A.P. McEnery, E. Cosgriff-Hernandez, Prevention of Oxygen Inhibition of PolyHIPE Radical Polymerization Using a Thiol-Based Cross-Linker, ACS Biomater Sci Eng. 3 (2017) 409–419, https://doi.org/10.1021/acsbiomaterials.6b00663.
[47] T.J. McKenzie, K. Rost, S. Smail, O. Mondain-Monval, T. Brunet, N. Ayres, Mechanically tunable PDMS-based polyHIPE acoustic materials, J Mater Chem C Mater. 10 (2022) 6222–6226, https://doi.org/10.1039/d2tc00136e.
[48] T.J. McKenzie, P.S. Heaton, K. Rishi, R. Kumar, T. Brunet, G. Beaucage, O. Mondain-Monval, N. Ayres, Storage Moduli and Porosity of Soft PDMS PolyMIPEs Can Be Controlled Independently Using Thiol-Ene Click Chemistry, Macromolecules. 53 (2020) 3719–3727, https://doi.org/10.1021/acs.macromol.0c00217.
[49] E. Lovelady, S.D. Kimmins, J. Wu, N.R. Cameron, Preparation of emulsion-templated porous polymers using thiol-ene and thiol-yne chemistry, Polym. Chem. 3 (2011) 559–562, https://doi.org/10.1039/c0py00374c.
[50] B. Sergent, M. Birot, H. Deleuze, Preparation of thiol-ene porous polymers by emulsion templating, React Funct Polym. 72 (2012) 962–966, https://doi.org/10.1016/j.reactfunctpolym.2012.02.011.
[51] J. Naranda, M. Sušec, U. Maver, L. Gradišnik, M. Gorenjak, A. Vukasović, A. Ivković, M.S. Rupnik, M. Vogrin, P. Krajnc, Polyester type polyHIPE scaffolds with an interconnected porous structure for cartilage regeneration, Sci Rep. 6 (2016) 1–11, https://doi.org/10.1038/srep28695.
[52] M. Sušec, S.C. Ligon, J. Stampfl, R. Liska, P. Krajnc, Hierarchically porous materials from layer-by-layer photopolymerization of high internal phase emulsions, Macromol Rapid Commun. 34 (2013) 938–943, https://doi.org/10.1002/marc.201300016.
[53] T.J. Wallin, L.E. Simonsen, W. Pan, K. Wang, E. Giannelis, R.F. Shepherd, Y. Mengüç, 3D printable tough silicone double networks, Nat Commun. 11 (2020) 4000, https://doi.org/10.1038/s41467-020-17816-y.
[54] P. Shen, S.Z. Moghaddam, Q. Huang, A.E. Daugaard, S. Zhang, P. Szabo, Hard-soft thiol-ene materials without interfacial weakness, Mater Today Commun. 21 (2019), 100657, https://doi.org/10.1016/j.mtcomm.2019.100657.
[55] G. Liu, Z. Ding, Q. Yuan, H. Xie, Z. Gu, Multi-Layered Hydrogels for Biomedical Applications, Front Chem. 6 (2018) 1–10, https://doi.org/10.3389/fchem.2018.00439.
[56] A.H. Aziz, J. Wahlquist, A. Sollner, V. Ferguson, F.W. DelRio, S.J. Bryant, Mechanical characterization of sequentially layered photo-clickable thiol-ene hydrogels, J Mech Behav Biomed Mater. 65 (2017) 454–465, https://doi.org/10.1016/j.jmbbm.2016.09.007.
[57] M.E. Smithmyer, S.E. Cassel, A.M. Kloxin, Bridging 2D and 3D culture: Probing impact of extracellular environment on fibroblast activation in layered hydrogels, AIChE J. 65 (2019) 1–14, https://doi.org/10.1002/aic.16837.
[58] A.A. Aimetti, A.J. Machen, K.S. Anseth, Poly(ethylene glycol) hydrogels formed by thiol-ene photopolymerization for enzyme-responsive protein delivery, Biomaterials. 30 (2009) 6048–6054, https://doi.org/10.1016/j.biomaterials.2009.07.043.
[59] C.R. Langford, D.W. Johnson, N.R. Cameron, Preparation of hybrid thiol-acrylate emulsion-templated porous polymers by interfacial copolymerization of high internal phase emulsions, Macromol Rapid Commun. 36 (2015) 834–839, https://doi.org/10.1002/marc.201400733.
[60] T.J. McKenzie, S. Smail, K. Rost, K. Rishi, G. Beaucage, N. Ayres, Multi-layered polymerized high internal phase emulsions with controllable porosity and strong interfaces, Polymer (Guildf). 231 (2021), 124116, https://doi.org/10.1016/j.polymer.2021.124116.
[61] M.M. Perera, N. Ayres, Gelatin based dynamic hydrogels: Via thiol-norbornene reactions, Polym Chem. 8 (2017) 6741–6749, https://doi.org/10.1039/c7py01630a.
[62] E. Pedraza, A.-C. Brady, C.A. Fraker, C.L. Stabler, Synthesis of Macroporous Poly (dimethylsiloxane) Scaffolds for Tissue Engineering Applications, J Biomater Sci

Polym Ed. 24 (2013) 1041–1056, https://doi.org/10.1080/09205063.2012.735097.Synthesis.
[63] M. Tomin, Á. Kmetty, Polymer foams as advanced energy absorbing materials for sports applications—A review, J Appl Polym Sci. 139 (2022) 1–23, https://doi.org/10.1002/app.51714.
[64] Z.J. Zhang, S.N. Fu, Shear Elastic Modulus on Patellar Tendon Captured from Supersonic Shear Imaging: Correlation with Tangent Traction Modulus Computed from Material Testing System and Test-Retest Reliability, PLoS One. 8 (2013) 1–9, https://doi.org/10.1371/journal.pone.0068216.
[65] G. Singh, A. Chanda, Mechanical properties of whole-body soft human tissues: A review, Biomed. Mater. (Bristol). 16 (6) (2021) 062004.
[66] A. Argun, U. Gulyuz, O. Okay, Interfacing Soft and Hard Materials with Triple-Shape-Memory and Self-Healing Functions, Macromolecules. 51 (2018) 2437–2446, https://doi.org/10.1021/acs.macromol.8b00233.